Density of states in $Bi_{12}TiO_{20}$ from time-of-flight measurements

2007 J. Phys.: Condens. Matter 19 476202

(http://iopscience.iop.org/0953-8984/19/47/476202)

IOP PUBLISHING JOURNAL OF PHYSICS: CONDENSED MATTER

J. Phys.: Condens. Matter **19** (2007) 476202 (20pp) doi:10.1088/0953-8984/19/47/476202

Density of states in $Bi_{12}TiO_{20}$ from time-of-flight measurements

C Longeaud[1], H Belgacem[2] and C Douay[1]

[1] Laboratoire de Génie Electrique de Paris, UMR 8507 CNRS, Ecole Supérieure d'Electricité, Universités Paris VI et XI, 11 rue Joliot Curie, Plateau de Moulon, 91190, Gif sur Yvette, France
[2] Laboratoire des Matériaux Semi-conducteurs et Métalliques, Faculté des Sciences et des Sciences de l'Ingénieur, Université Mohamed Khider, BP 145, 07000 Biskra, Algeria

E-mail: longeaud@lgep.supelec.fr

Received 25 May 2007, in final form 27 September 2007
Published 31 October 2007
Online at stacks.iop.org/JPhysCM/19/476202

Abstract

Two sillenite crystals of $Bi_{12}TiO_{20}$, one intrinsic and one lead doped, have been studied by means of the time-of-flight (TOF) experiment. After a short presentation of the technique, we return to the different methods proposed to extract the transit time from the current transients recorded with the TOF experiment. Further, we illustrate the possibility of extracting the density of states from these transients by means of a Laplace transform applied to the variation with time of the transient currents. Then we present some experimental results. The room temperature drift mobilities we measured were equal to 2 and 0.2 $cm^2\ V^{-1}\ s^{-1}$ for the lead doped and intrinsic sample, respectively. Finally we present the densities of states found for each crystal and compare them to the results obtained from modulated photocurrent experiments applied to the same samples.

(Some figures in this article are in colour only in the electronic version)

1. Introduction

Many methods developed to investigate the transport properties of highly resistive semiconductors are based on the photoconductive properties of these materials [1]. Among these techniques the time-of-flight (TOF) technique, proposed decades ago by Spear [2], has been largely applied since then to a large variety of materials such as semi-insulating crystals [3–5], amorphous semiconductor thin films [6, 7], chalcogenides [8, 9] and polymers [10, 11]. First developed to deduce both hole and electron mobility values, for it gives the opportunity to choose the type of carriers drifting through the sample, it was later considered as a mean to deduce more information on the material properties such as the defect densities of localized states present in the gap. Various models of transport and interactions of carriers with trapping states have been elaborated (continuous time random walk [12], or multiple trapping [13–15]) mostly for crystalline or disordered semiconductors, whereas transport models in polymers

are still a matter of debate [11]. At the same time several methods were proposed to extract the density of states (DOS) of the probed materials from an analysis of the recorded transients [16–18]. As far as the determination of the DOS of a given semiconductor is concerned, other methods have also been suggested simultaneously with those proposed for TOF. Among these the transient photocurrent (TPC) technique is close to the TOF method, the main difference consisting in the geometry of the sample fitted with coplanar electrodes instead of sandwich ones. It was shown that data treatment by means of a Fourier transform [19] or a Laplace transform [20] could indeed elicit some information about the semiconductor DOS.

In this paper we present TOF measurements performed on sillenite crystals $Bi_{12}TiO_{20}$ (BTO). The sillenites ($Bi_{12}XO_{20}$, BXO with X = Si, Ti, Ge) are photorefractive materials with potential technological applications in holographic storage or optical switching and filtering, among others. To our knowledge BGO and BSO have received more attention [3, 4] than BTO, for which we found only a few reports in the literature [5]. We first present experimental details of the TOF experiment as we have performed it and return to the various treatments of the transients proposed in the literature to extract as much information as possible from these. In a second step, we present some results of the simulation of the TOF experiment as well as of the transient photocurrent technique we have developed. These simulations will be used both to show that TPC and TOF in the pre-transient regime give rise to the same transient behaviours as already suggested by Main [19] and to introduce the technique we have defined to extract the DOS of a semiconductor from the TOF transient.

A third part is dedicated to experimental results, and we underline some of the problems we had to face with the considered BTO crystals. Finally we present the DOS we have extracted from our method and compare these results with the results of the modulated photocurrent (MPC) technique performed on the same crystals [21].

2. Experimental details

2.1. Samples

Two types of sample were studied. An intrinsic BTO (BTO-J18) and a Pb doped BTO ($Bi_{12}Ti_{0.9}Pb_{0.1}O_{20}$, BTO:Pb). The crystal thicknesses were 0.8 mm and they were fitted with two stripes of evaporated aluminium on each face, one being semi-transparent with a transmission of the order of 70% for the BTO-J18 and 50% for the BTO:Pb at the wavelength of the laser (337 nm). All the samples of this study were grown in the same laboratory in Brazil using the same procedure and raw materials [22].

2.2. Experiment

We present in figure 1(a) a simple scheme of the TOF technique. The sample of thickness L sandwiched between two electrodes, one being semi-transparent, is biased with a polarization V_{dc}. A short (3 ns) flash of light from a nitrogen laser ($\lambda = 337$ nm) absorbed at the surface of the sample results in carrier generation at one face of the crystal. The sign of the bias applied on the semi-transparent electrode determines the sign of the carriers that drift through the sample toward the other face (in figure 1(a) the electrons). The drift of these electrons generates a transient current outside the sample, the intensity of which is measured via the amplification of the voltage drop in a resistor R. From the time evolution of this current, recorded on an oscilloscope, one can deduce a transit time t_t, i.e. the time the carriers take to cross the whole thickness of the sample. We shall come back to the analysis of this transient later and we are going to concentrate first on the details of the measurement technique itself.

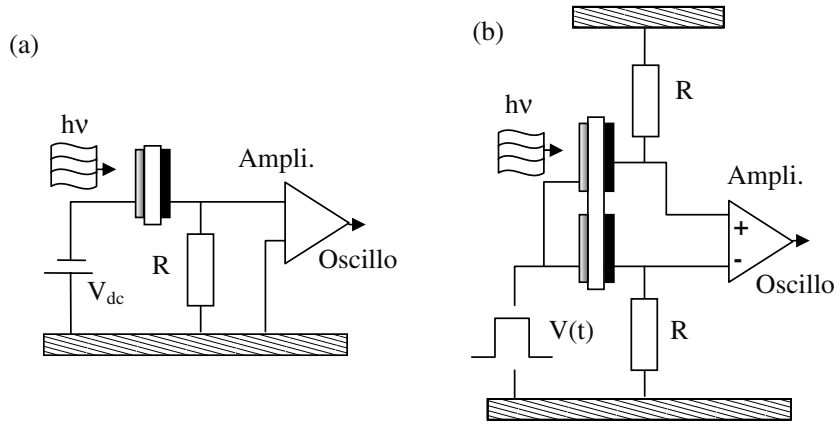

Figure 1. (a) Simple scheme showing the basic set-up for transient recording in the TOF experiment and (b) a description of the set-up we used for transient recording. The differential amplification of the signals minimizes the overshoots due to the application of pulsed bias to the samples.

The TOF technique requires a uniform field ξ both in time and in space. Indeed, the recorded transient must be that of the drifting carriers and not linked to some evolution with time of the applied field. Moreover, if the field is not uniformly distributed in space the carriers will not drift at a constant speed and will not even go through the sample at all. Generally, the electrical contacts deposited on both sides of the sample are not strictly ohmic. Actually, it is preferable that these contacts are blocking contacts so as to avoid carrier injection by the applied field in addition to the carriers injected by the flash of light. Hence, on applying a dc voltage to the sample the field distributes between the contacts and its uniformity through the whole thickness is highly questionable after a time larger than the dielectric relaxation time (τ_r) of the crystal. One possible way to obtain a uniform field is to apply a voltage pulse to the sample and to record the current transient before the dielectric relaxation occurs. However, due to the thickness of the crystal, one has to apply rather a high voltage pulse to fulfil this condition—a transit time shorter than τ_r—and these could damage the electronic circuit used to record the transient current because of the overshoots that occur at the onset and end of the bias pulse.

To overcome this difficulty we have used two pairs of identical contacts deposited on the same crystal to obtain the same capacitance, the voltage pulse being applied to both pairs. The same R was used for each pair of contacts and one of them was kept in the dark. By differentially amplifying the responses of each pair we got rid of the overshoots at both ends of the voltage pulse and recorded only the current transient linked to the flash of light (see figure 1(b)).

A synchronization between the voltage pulse and the light pulse is achieved in such a way that the time elapsed between the onset of the bias and the flash of light is shorter than τ_r. Typically, in the case of the crystals we measured, presenting values of τ_r of the order of a few seconds at room temperature, the rise time of the bias pulse was of the order of 0.1 ms and the time between the beginning of the voltage pulse and the flash of light as well as the voltage pulse duration were chosen to be of the order of a millisecond. The transients measured were always such that the total time elapsed after the bias application was lower than τ_r.

Another source of modification of the applied field is the accumulation of charges in the traps of the band gap creating a local field competing with the applied one. To prevent such a problem we have always worked with a very low flux of light. The energy of the laser pulse

reaching the sample was attenuated by neutral density filters down to values of the order of 1 μJ per pulse. In addition, the pulse of light was shone onto the sample every 60 bias pulses, the repetition frequency of the latter being 0.8 Hz. Under this condition we assumed that the slowest carriers generated by a laser pulse, i.e. those whose drift is limited by the deepest traps, were swept out of the sample by the 60 successive bias pulses applied without any light prior to the next flash of light.

We have always used rather low R, the maximum value of which was equal to 12 kΩ. With this value the response time of the circuit, which has to be shorter than the transit time, was of the order of 30 ns, far smaller than the transit times we measured, the lowest ones being of the order of a few μs.

2.3. Treatment of the results

One point of controversy concerns the method used to derive the transit time from the experimental data. In the following our analysis will be mainly based on the multiple trapping model in which carriers are successively trapped and released while drifting through the material. Let us recall that two main types of transit can be observed. In the first type of transit one observes that after a fast drop of the current at very short times, a plateau is clearly visible followed by a fast decrease of the current toward zero. The basic interpretation of such a curve is that immediately after generation the carriers are trapped and recombine at the generation interface (the first fast drop). Then, despite the trapping and release events, carriers remain gathered into a packet while drifting through the sample (the plateau), a packet that can spread under the influence of diffusion for instance, until they reach the back electrode where they recombine (the final fast decrease). This type of transit is called non-dispersive, for it is easy to derive a mean transit time t_t for all the carriers by choosing for instance the time at which the current value equals half the plateau value. Intuitively one can attribute this time to the arrival of approximately half the total number of drifting carriers and there is only very little dispersion in the transit time of the carriers. The drift mobility μ_d of the carriers is then easily deduced from the relation $t_t = L/\mu_d\xi$.

Problems in the determination of the transit time arise mainly with the second type of transit in which no plateau can be observed but a steady decrease instead. However, a logarithmic plot of the transient current as function of the logarithm of time usually reveals two slopes corresponding to two different regimes. The first slope, the lowest, characterizes a spreading of the carriers through the whole sample mostly due to heavy trapping and slow release. This is the pre-transit regime. The second slope, the steepest, is attributed to the eventual exit of the carriers (post-transit regime). This behaviour is due to a large dispersion of the times of arrival of the carriers at the back electrode, hence the name of dispersive transport. Different methods have been proposed to estimate a transit time from such a curve, mostly based on graphical techniques. The simplest one consists in drawing two tangents to the $I(t)$ curve plotted in a log–log scale and to take the time of their intersection as the transit time. More sophisticated is the idea to plot a parallel of the first tangent a factor of ln(2) below and to take the transit time as the time it intersects the second tangent. In the case of hydrogenated amorphous silicon, Vanderhaghen [23] has shown that this time corresponded roughly to the arrival of half the injected carriers into the sample. However, more recently an even more sophisticated technique has been proposed based on the analysis of many dispersive transits [24]. It consists in a fit of the observed transient by a function taking into account the dispersivity of the transient. This function $s(t)$ is the product of the current that would flow through an infinite sample by a function $s_0(t)$ taking account of the distribution of arrival times of the carriers at the collecting electrode.

Scott *et al* have essentially worked on polymers but their transients approach was also applied to TOF measurements performed on $Bi_{12}GeO_{20}$ (BGO) and $Bi_{12}SiO_{20}$ (BSO) by Bloom *et al* [4] with a modification of the expression of the pre-factor $s_0(t)$.

Since the fitting function has to be adapted to a given material one can wonder about the universality of such a procedure. Actually, the term that has to be modified is the one describing the transient before collection and recombination of the carriers at the back electrode, that is the pre-transit regime. This regime, as we will show below, is strongly linked to the density of states (DOS) present in the material and limiting the electron drift by the trapping and release process. Therefore, it is not surprising that the pre-factor $s_0(t)$ is sample dependent.

This behaviour can also be shown by very simple considerations and comparison with another transient technique. Let us consider for instance a transient of electrons presenting a concentration in the extended states $n(x, t)$, x being the space coordinate taken from the generation electrode and t the time, one has the relation (see for instance [17])

$$RC\frac{\mathrm{d}I(t)}{\mathrm{d}t} + I(t) = \frac{S}{L}q\mu_n\xi\int_0^L n(x,t)\,\mathrm{d}x, \tag{1}$$

in which C is the sample capacitance, R the measurement resistor, $I(t)$ the current in the external circuit, q the absolute value of the electron charge, μ_n the electron extended states mobility and S the illuminated area of the sample. This expression is valid only when no carriers, or only a very small proportion of them, have reached the recombination electrode, that is in the pre-transit regime. It is also valid at any time of the transit if the diffusion influence can be neglected. If one chooses a very small R or works with a current–voltage amplifier, the input impedance of which virtually equals 0, this expression reduces to

$$I(t) = \frac{S}{L}q\mu_n\xi\int_0^L n(x,t)\,\mathrm{d}x. \tag{2}$$

It means that the carrier distribution in the sample has no influence on the external current and that the whole system behaves exactly as in the case of a transient photocurrent (TPC) experiment [25, 26]. This latter experiment is performed with a sample in coplanar geometry. After a dc bias is applied, the sample is illuminated in between the electrodes by a short pulse of light, usually as short as the one used for TOF. The distance between the two electrodes is chosen to be large enough so as to neglect the very small loss of carriers at one of the electrodes due to their drift toward it. The current in the external circuit is thus completely dominated by the trapping and release events as is the case in the pre-transit regime of the TOF experiment. In the case of the TPC it was shown that, by means of a Fourier transform of the transient photocurrent, it was possible to deduce the density of states of the studied material [19]. More recently Main *et al* [27] demonstrated that the recombination of carriers during the TPC measurement has almost no influence on the DOS determination from a Fourier transform of the TPC signal.

Other authors have proposed the use of a Laplace transform instead of a Fourier transform, the basic treatment of the transient signal being very similar as with a Fourier transform [20]. Following the work of these authors, it is precisely a Laplace transform that we have applied to the recorded transients in the TOF experiment to determine the DOS interacting with free carriers during their transit, as will be shown below.

To complete discussion on the possible treatments of transient photocurrents we have to mention that the case of the post-transit was treated by Seynhaeve *et al* [18], and they showed that the density of states was proportional to the product $tI(t)$ under the assumption that all traps at a given depth release the carriers at the same time, an assumption that may not be satisfied in the case of very thick samples.

From these theoretical considerations we can draw the following conclusions. Though the graphical technique seems to be too simplistic it remains to our knowledge the only method for extracting the transit time value with a minimum of assumptions. In addition, this technique can be applied independently of the nature of the transit (dispersive or not). As mentioned above, the transient shape in the pre-transit regime is connected to the DOS of the sample and one can derive this DOS from the Fourier or Laplace analysis of the TOF current. However, if one limits its investigation to the observation of the beginning of the TOF transient, as is the case when studying the drift mobility, this method is limited by the small range of time taken into account compared to the decades of time recorded during a TPC experiment. Hence, acquisitions of different transient curves at different temperatures are necessary to achieve a DOS spectroscopy over a rather large energy range.

In the next section we will illustrate these conclusions by means of numerical simulations.

3. Numerical simulations

We have performed numerical simulations of the TOF and TPC experiments. To avoid heavy mathematical presentation we shall present the basic equations used in these simulations considering a single trapping state of density $N(E)$, E being the energy. In the dark we shall write the densities of free electrons and holes, and the occupation function as n_0, p_0 and f_0, respectively, and after illumination the same quantities will be denoted without the index 0. The excess of electrons (holes) will be equal to $n - n_0$ ($p - p_0$) whereas the excess of trapped carriers will be equal to $N(f - f_0)$. With these notations the continuity equations are

$$\begin{aligned}
\frac{\partial (n - n_0)}{\partial t} &= G_n \delta(t) \\
&\quad + \int_E \left[-C_n (n - n_0) N (1 - f) + (e_n + C_n n_0) N (f - f_0) \right] \mathrm{d}E + \frac{1}{q} \frac{\partial J_n}{\partial x} \\
\frac{\partial (p - p_0)}{\partial t} &= G_p \delta(t) \\
&\quad + \int_E \left[-C_p (p - p_0) N f - \left(e_p + C_p p_0 \right) N (f - f_0) \right] \mathrm{d}E - \frac{1}{q} \frac{\partial J_p}{\partial x} \\
\frac{\partial N (f - f_0)}{\partial t} &= C_n (n - n_0) N (1 - f) - C_p (p - p_0) N f \\
&\quad - \left(e_n + e_p + C_n n_0 + C_p p_0 \right) N (f - f_0)
\end{aligned} \tag{3}$$

in which C_n (C_p) is the capture coefficient for electrons (holes) and e_n (e_p) the emission rate of electrons (holes) from the trap toward the conduction (valence) band. J_n and J_p are the electron and hole current densities, respectively, depending on time t and x, the distance from the generation electrode. G_n (G_p) is the generation rate of electrons (holes) at the generation electrode at $t = 0$, the $\delta(t)$ function accounting for the very short duration of the pulse of light in the TOF or TPC experiments. In these equations the quantities n, p and f are also functions of x and time. In addition, the occupation functions f and f_0 depend on the energy position E in the gap as well as N. The integrals are taken over the whole gap but can be restricted to the energy range in which N extends. The last equation is verified at each energy level.

We have also taken into account a possible evolution of the field due to the space charge effect by calculating the derivative of the applied field with respect to x taking account of the local charge density.

Two simulation codes were developed to solve these equations, one for each experiment, the TPC and the TOF. In each code we solve these equations taking discrete steps of time, energy and, for TOF, distance. For the TPC the number of 'photo-created' carriers is so

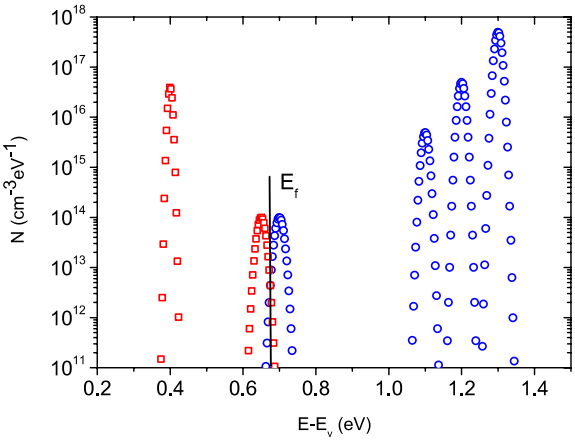

Figure 2. Density of states in the gap of a virtual semiconductor that we have introduced in our simulations of TPC and TOF. The position of the Fermi level is indicated by a vertical line.

low that one can assume that the terms containing $(f - f_0)$ can be neglected. In addition the 'experiment' is performed under conditions such that the current densities are uniform, which implies that the derivatives according to x are null. It is possible then to build a matrix M, the elements of which correspond to one step of time Δt, and multiplying the vector $[n(t = 0), p(t = 0), f(E_1, t = 0), \ldots, f(E_i, t = 0), \ldots, f(E_k, t = 0)]$ by M gives the vector $[n(\Delta t), p(\Delta t), f(E_1, \Delta t), \ldots, f(E_i, \Delta t), \ldots, f(E_k, \Delta t)]$. The product of M by itself (M^2) will correspond to a step of $2\Delta t$, the product of M^2 by itself to $4\Delta t$, etc. Starting with a very short Δt, fixed to a tenth of the lowest time constant of the system, one can easily reach very long times of the order of a second, since by repeating the above procedure n times 1 ends with a time equal to $2^n \Delta t$. For the TOF the resolution must be made step by step because the carriers are 'photo-created' in the first slice of width Δx of the sample and it is not possible to assume that the current densities are uniform. This step by step method, starting with a very short Δt, fixed as in TPC by the shortest time constant, gives rise to a rather long calculation.

We present in figure 2 the density of states we have introduced in our simulations. The virtual semiconductor we considered has a gap of 1.5 eV. The equivalent densities of states at the bottom of the conduction band and at the top of the valence band were both taken equal to 2.5×10^{19} cm^{-3} at 300 K. The Fermi level is pinned around the middle of the gap ($E_f - E_v = 0.675$ eV) by two peaks of states: one donor peak ($N_{max} = 10^{14}$ cm^{-3} eV^{-1}, $E_{max} - E_v = 0.65$ eV and a standard deviation $\sigma = 10$ meV, open squares) and an acceptor peak ($N_{max} = 10^{14}$ cm^{-3} eV^{-1}, $E_{max} - E_v = 0.70$ eV, $\sigma = 10$ meV, open circles). Three peaks of acceptor states (open circles) are located in the upper part of the gap ($N_{max} = 5 \times 10^{17}$ cm^{-3} eV^{-1}, $E_{max} - E_v = 1.3$ eV; $N_{max} = 5 \times 10^{16}$ cm^{-3} eV^{-1}, $E_{max} - E_v = 1.2$ eV; $N_{max} = 5 \times 10^{15}$ cm^{-3} eV^{-1}, $E_{max} - E_v = 1.1$ eV, with the same standard deviation $\sigma = 8$ meV) and a single peak of donor states (open squares) is set at $E_{max} - E_v = 0.4$ eV with a maximum $N_{max} = 4 \times 10^{16}$ cm^{-3} eV^{-1} and $\sigma = 5$ meV. The capture coefficients for holes and electrons were taken identical for all the states, $C = 10^{-8}$ cm^3 s^{-1}, and the mobilities of the electron and hole extended states equal to $\mu_n = 100$ cm^2 V^{-1} s^{-1} and $\mu_p = 0.1$ cm^2 V^{-1} s^{-1}, respectively. Considering these values, the calculated TOF and TPC transients were related to electron currents flowing in the 'sample'. For the TOF simulation 200 distance steps, 250 energy steps and up to 10^7 time steps where used. These time steps were

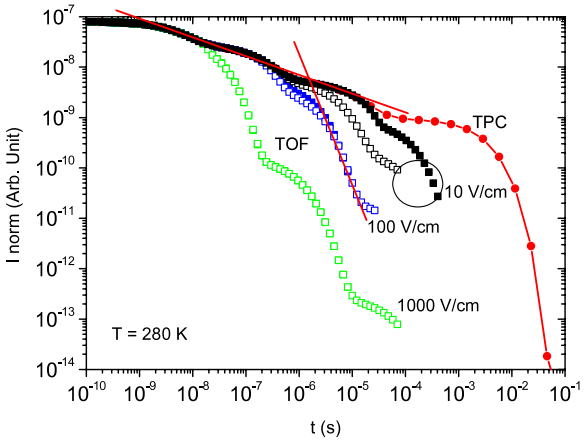

Figure 3. Typical transients obtained from our simulations of TPC (line + full circles) and TOF including diffusion (open symbols) or without diffusion (full symbols). The fields at which the TOF was calculated are indicated in the figure.

adapted during calculation so as to be lower than the fastest time constant of the system. For the TPC, 500 energy steps were used.

We present in figure 3 the currents of the transients calculated at $T = 280$ K, normalized to the same value at short time, obtained in both simulations. The TPC transient (line + full circles) can be explained as follows. At short time the current is constant since the time is shorter than the trapping time constant fixed by all the empty trapping states. Then a first drop appears around $t = 5$ ns, corresponding to electron trapping in all the empty states of the gap. As time goes on some electrons are released ($10^{-8} < t < 10^{-7}$ s) by thermal emission from the upper peak of acceptor states (at 1.3 eV below E_c) slowing down the current decrease. Electrons emitted from this upper peak redistribute into the trapping states, mostly in the deeper ones, their thermal emission time constant being much lower since the emission rate depends exponentially on the energy gap between the defect peak and the extended states band. When almost all the electrons have been emitted from the upper acceptor states the current resumes its decrease until emission for the next acceptor states (at 1.2 eV below E_c) slows down this decrease again ($10^{-6} < t < 10^{-5}$ s). This process repeats for the last acceptor peak (at 1.1 eV below E_c) and ends with an eventual rapid drop of the current due to deep trapping of electrons in the states close to the Fermi level and recombination.

The TOF simulations were performed with different 'applied' fields, the values of which are reported in figure 3. These simulations were performed taking account of the carrier diffusion (open symbols) or not (full symbols). For the different applied fields the currents were normalized to the TPC current for an easy comparison. For 10 V cm^{-1} the TOF current evolution follows exactly the TPC results on a very long time range simply because the field is so low that the electrons reach the back electrode after quite a long time spent in the 'sample'. It confirms that, indeed, TOF and TPC currents behave in exactly the same way while the carriers injected in TOF remain in the 'sample'. Obviously, for higher applied fields, the TOF curves depart from the TPC one at shorter times: the higher the field the shorter the time of this departure. However, structures are still visible on these TOF curves after the transit time, corresponding to an influence of the defect states on these transients by emission of carriers during the post-transit regime. The influence of the diffusion is clearly seen on the curve calculated with a field of 10 V cm^{-1}. It is less pronounced on the curve simulated with

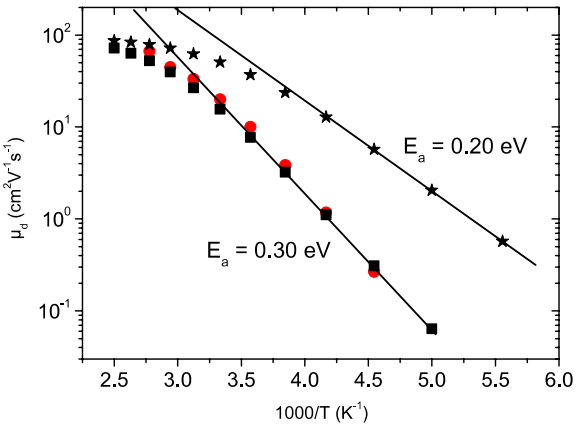

Figure 4. Arrhenius plot of the drift mobility determined graphically (circles) or extracted from the simulation (squares) performed with an applied field of 100 V cm^{-1}, and extracted from the simulation performed with an applied field of 1000 V cm^{-1} (stars).

100 V cm^{-1} and almost negligible for the curve simulated at 1000 V cm^{-1}. It shows that for low fields the carrier diffusion speeds up their transit through the sample by spreading the carrier packet widely. For all the simulated transits we have chosen to define the transit time t_t as the time for which half the injected carriers have reached the back electrode. This time can be easily extracted during the simulation by calculating at each step the number of remaining carriers both in the band and in the traps. At low field (10 V cm^{-1}) the transit time is particularly dependent on the diffusion since it decreases by a factor of 10 from 120 μs without diffusion to 11 μs if we take account of the diffusion. With 100 V cm^{-1} it drops from 2.6 to 2 μs and the difference between the transit times is insignificant at 1000 V cm^{-1} ($t_t = 54$ ns). It can be noted that, even if one does not take the diffusion into account, the product $t_t \times \xi$ is far from being constant, indicating that our simulations reproduce dispersive transients at 280 K. In figure 3 we have plotted the mean slopes of the current decreases before and after the transit time. From their intersection we deduce a 'transit time' of the order of 1.5 μs, a value not far from the one extracted from the simulation. Hence, though not very rigorous, the 'graphical' method is still a good mean to obtain a good order of magnitude of the carrier transit time with a minimum of assumptions.

We present in figure 4 the evolution with temperature of the drift mobility μ_d extracted numerically from the simulations performed with an 'applied field' of 100 V cm^{-1} (squares), extracted graphically with the two tangents method (circles) applied to the transits calculated with 100 V cm^{-1} and evolution of μ_d extracted numerically from the simulations performed with an 'applied field' of 1000 V cm^{-1} (stars).

In the case of 100 V cm^{-1}, at low temperature the drift mobility is activated with an energy $E_a = 0.3$ eV, indicating that the transit is essentially limited by the defect located at 0.3 eV below the conduction band. It can also be seen in figure 4 that the drift mobility values extracted graphically from the simulated transient (circles) match rather well with the 'exact' values determined with the simulation (squares). With an 'applied field' of 1000 V cm^{-1} the activation of the drift mobility is only 0.2 eV, showing that the transients are limited essentially by the defect level located at 0.2 eV below E_c.

Taking account of the shape of the transients at low temperature (figure 3) and of the activation of the drift mobility in the range of temperature the transits would be described as dispersive, whereas at higher temperature the transport turns out to be less and less dispersive

with increasing temperature. As the temperature increases the emission of carriers from the traps is activated and their influence on the transit weakens. As a consequence, the drift mobility increases toward the extended states value of the mobility (100 $cm^2\ V^{-1}\ s^{-1}$).

We want to underline that these behaviours are not universal. In particular, the measured activation energy of μ_d may not be linked to any particular peak of states [28]. Indeed, one can observe that the drift mobility is activated with temperature even in material in which there are no defect peaks but a continuous distribution of states. For instance, the study of the conduction band tail states in hydrogenated amorphous silicon leads to an activation energy of, say, 0.14 eV. At this energy position the band tail does not present any peak at all but is rather steadily decreasing toward mid gap. Moreover, a change in the slope of the activation energy of the drift mobility can also be due to a shift with temperature from one predominant defect state limiting the transport to another one. It is an eventual determination of the density of states from the TOF transients that allow a choice to be made between these different possibilities.

We have tested the possibility of deducing the density of states interacting with the drifting carriers by means of a Laplace transform applied to several simulated transients following the work of Nagase *et al* [20] with a Tikhonov regularization.

Neglecting the hole contribution as well as the influence of the diffusion, and assuming that the field is uniform through the sample and that the DOS is made of m discrete levels of states, the system (3) transforms into [20, 29, 30]

$$\frac{\partial n\,(x,t)}{\partial t} = -\sum_{i}^{m} \frac{\partial n_i\,(x,t)}{\partial t} - \mu_n \xi \frac{\partial n\,(x,t)}{\partial x} + G_n \delta\,(t), \tag{4}$$

$$\frac{\partial n_i\,(x,t)}{\partial t} = \omega_i n\,(x,t) - \gamma_i n_i\,(x,t)\,, \tag{5}$$

where $\omega_i = C_n N(E_i)\Delta E$ and $\gamma_i = e_n(E_i) = C_n N_c \exp(-E_i/k_B T)$ are, respectively, the capture and release rates of electrons at the energy level $E_i = i\Delta E$ the ith energy level below the mobility edge. N_c is the equivalent density of states at the bottom of the conduction band, k_B is the Boltzmann constant and T is the measurement temperature. The product $C_n N_c$ is often written as ν_n, an attempt-to-escape frequency. The generation can be written as $G_n = n_{00}\delta(x)$, the $\delta(x)$ function taking account of the fact that the carriers are generated in a very thin slice on top of the sample.

Equations (4) and (5) can be solved using Laplace transform giving rise to

$$\hat{I}(s) = Sqn_{00}\frac{1-\exp\left[-a(s)t_0\right]}{a(s)t_0}, \tag{6}$$

the expression of $a(s)$ being the same as in equation (2.16) of [20]. Finally one has

$$\sum_{1}^{m} \frac{\gamma_i C_n N(E_i)\Delta E}{\left[s+\gamma_i\right]^2} = \frac{Sqn_{00}}{st_0 B\,(s)} \frac{\mathrm{d}}{\mathrm{d}\ln\,(s)}\left[\frac{1}{\hat{I}\,(s)}\right] - 1, \tag{7}$$

from which a localized-state distribution can be obtained numerically from its resolution, the expression of $B(s)$ being the same as in equation (2.22) of [20].

The Laplace transform of $I\,(t)$ can be carried out by simple numerical integration over N sampling points:

$$\hat{I}\,(s) = \sum_{j=2}^{N-1} I\,(t_j)\mathrm{e}^{-t_j s}\left(t_{j+1} - t_{j-1}\right)/2. \tag{8}$$

To determine $B(s)$ the following simple procedure is used: (i) Sqn_{00} can be determined by extrapolating $\hat{I}(s)$ toward $s = 0$, (ii) the values of $a(s)t_0$ are obtained by numerically solving

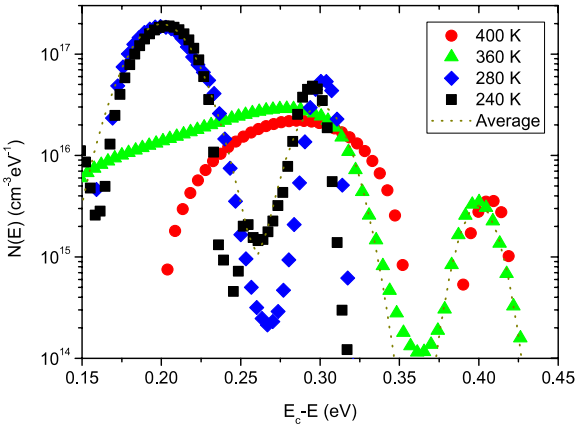

Figure 5. Densities of states (symbols) deduced from a Laplace transform applied to transits simulated at different temperatures displayed in the figure. An average DOS (dotted line) was deduced from these.

equation (6) using the values of $\hat{I}(s)$ and Sqn_{00} and (iii) $B(s)$ is determined by substituting $a(s)t_0$ into its expression.

We show here that it is possible to avoid the differentiation of equation (7). Let us consider the Laplace transform of $J(t) = tI(t)$, which is

$$\hat{J}(s) = \int_0^\infty tI(t)\mathrm{e}^{-st}\,\mathrm{d}t = -\frac{\mathrm{d}\hat{I}(s)}{\mathrm{d}s}. \tag{9}$$

$\hat{J}(s)$ is obtained in the same way as $\hat{I}(s)$ (see equation (8)). Using equation (9), equation (7) becomes

$$\sum_1^m \frac{\gamma_i C_n N(E_i)\Delta E}{\left[s+\gamma_i\right]^2} = \frac{Sqn_{00}}{t_0 B(s)}\frac{\hat{J}(s)}{\hat{I}(s)^2} - 1. \tag{10}$$

Equation (10) is a Fredholm integral equation of the first kind, and the density of states $N(E_i)$ is calculated in terms of Tikhonov regularization [31]. $I(0) = Sqn_{00}/t_0$ can be estimated from the extrapolated value of $I(t)$ toward $t = 0$, and n_{00} by the measurement of the injected charge via a calibrated photodiode.

We present in figure 5 the density of states that can be deduced from the simulated transients treated as if they were experimental. Several temperatures had to be used for the influence of the defect states interacting with the extended states and limiting the transients depends largely on temperature. At low temperatures only the peaks closer to the conduction band are revealed. At higher temperatures the response of these peaks is too fast to be properly resolved into well defined structures and only a broad contribution can be deduced. However, the deepest peak is well detected and reproduced. The final DOS equation is

$$N(E) = N_{\max 1}\exp\left[-\frac{(E-0.2)^2}{2\sigma_1^2}\right] + N_{\max 2}\exp\left[-\frac{(E-0.3)^2}{2\sigma_2^2}\right] + N_{\max 3}\exp\left[-\frac{(E-0.4)^2}{2\sigma_3^2}\right] \tag{11}$$

with $N_{\max 1} = 2.0 \times 10^{17}$ cm^{-3} eV^{-1}, $N_{\max 2} = 3.13 \times 10^{16}$ cm^{-3} eV^{-1}, $N_{\max 3} = 3.23 \times 10^{15}$ cm^{-3} eV^{-1}, $\sigma_1 = 17.5$ meV, $\sigma_2 = 13.8$ meV and $\sigma_3 = 10.3$ meV. One has to note that in

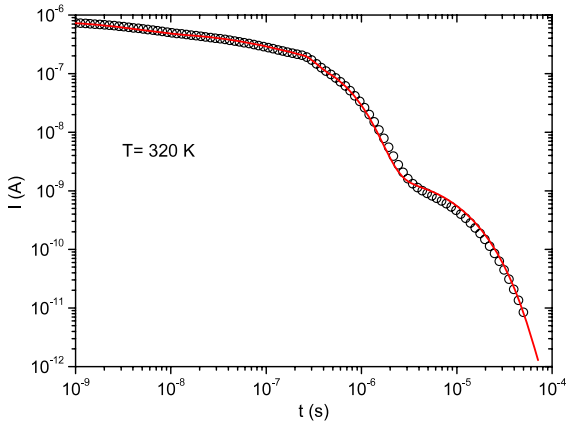

Figure 6. Calculation of the transient current (open circles) applying an inverse Laplace transform method with the deduced density of states presented in figure 5. This transient current calculated for $T = 320$ K compares rather well with the 'experimental' one given by our numerical simulation (full line).

the DOS equation (11) the energy reference was taken at E_c. The values of the maxima of the DOS peaks are close to those introduced in the simulation, whereas the values of the standard deviations σ are rather high, up to a factor of two too large compared to the values introduced in the simulations. However, it shows that theoretically the DOS can be extracted from the transients rather accurately.

This result is confirmed by calculation of computer-generated TOF transient photocurrents for a given localized states distribution using a numerical inverse Laplace transform technique [32]. The Laplace transform of the TOF current is obtained by numerically solving the Laplace transform of the basic equations (4) and (5). One obtains $\hat{I}(s)$ from equation (6) and from the $a(s)$ expression, and the variations of the current with time are deduced from the inverse Laplace transform of $\hat{I}(s)$

$$I(t) = \frac{1}{2\pi j} \int_{c-j\infty}^{c+j\infty} \hat{I}(s) e^{st}\, ds. \tag{12}$$

Introducing the previously deduced density of states (equation (11)) into such a calculation we have derived a transient current shape at $T = 320$ K that compares rather well with current variations obtained from our simulation performed for the same temperature (see figure 6).

The accuracy of this reconstruction of the simulated current by means of an inverse Laplace transform has been checked by varying the different parameters of the equation (11). The reconstructed current clearly departs from the simulated one if parameters like the maximum density of states are varied by a factor of say 2. Along with the discrepancy we observed for the standard deviations we determined it gives an order of magnitude of the errors that could be made when dealing with experimental data.

4. Experimental results

4.1. Determination of the drift mobility

We present in figure 7 a typical electron transient obtained on the intrinsic sample (BTO-J18) at room temperature with an applied bias of 400 V. The current is steadily decreasing with time and no special feature indicates the occurrence of a transit. Plotted in a log–log scale

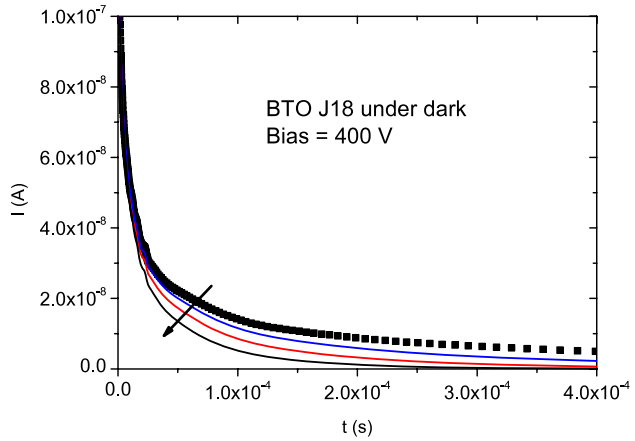

Figure 7. Transient recorded in the dark on the intrinsic BTO with 400 V applied (symbols). The lines and the arrow indicate the transient evolution when successive flashes of light are shone onto the sample at the same frequency as the bias pulses.

the same transient also decreases steadily with no particular break in the slope. Clearly, in the dark no transient is observable. Moreover, if the flash of light is applied synchronously with each bias pulse the successive transients decrease faster and faster as indicated in figure 7 until only a very sharp and fast transient signal is recorded. If the flash of light is applied every 60 bias pulses, following the same procedure as the one described in the previous section, this behaviour disappears but still no transit time could be observed (no clear break in the slope of the decreasing transient current). Such a behaviour was observed on both samples. In addition, such a test was repeated at different temperatures on both samples without any improvement in the transit time detection. We concluded that no carrier transit could be observed when the samples were maintained in the dark.

This behaviour is probably due to heavy trapping of the carriers during their drift into deep traps with a very slow release constant. It results in the disappearance of the carriers as if they recombine. Besides, the fact that the recorded current drops faster and faster after successive illumination probably indicates that a space charge is building close to the generation electrode resulting in a field that counter-influences the applied one. This type of problem has already been encountered in sillenites like $Bi_{12}GeO_{20}$ (BGO) [3], and these authors shown that by superimposing a continuous light of wavelength less than 550 nm to the flash of light used for carrier generation it was possible to record nice quasi-non-dispersive transits.

Hence we have tested the influence of the superimposition of continuous light provided by light emitting diodes with different peak emission wavelengths (640, 525, 450 and 385 nm). Figure 8 summarizes the results we obtained. The best transits were obtained under blue (450 nm) or green light (525 nm) with a shape resembling what one would expect in the case of transit on the edge between dispersive and non-dispersive behaviour. There was almost no difference between dark and red illumination for which the transient intensities were both low and continuously decreasing. The UV light (385 nm) did not help us either to observe 'nice' transits.

Our explanation is the following. The gap of BTO is of the order of 3.2 eV and on the studied samples we measured an activation energy of the order of 0.9 eV. BTO is supposed to be p-type in the dark which means that the dark Fermi level is 0.9 eV above the valence band. In the dark the generated electrons are probably deep trapped into levels in between the conduction band and the Fermi level. These traps are so deep that the release time is extremely

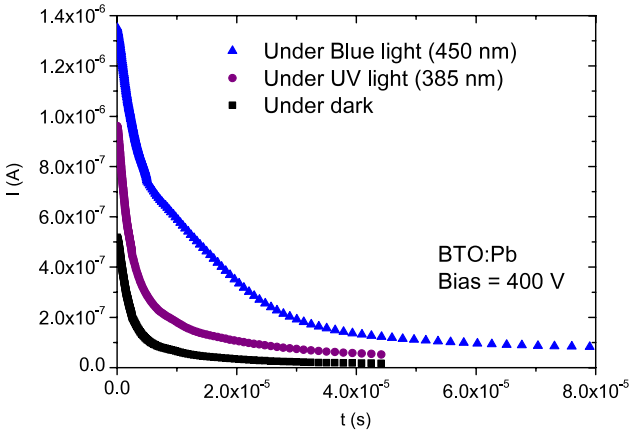

Figure 8. Transients observed without (dark) or with the superimposition of continuous light of various wavelength. It is under blue light that we obtained a signal that is the closest to what could be expected as a transient of electrons.

long and the carriers can be considered as lost for the transit. When one shines blue or green continuous light onto the sample the photon energy, 2.75 eV for the blue and 2.36 eV for the green, is such that electrons can be pumped from the occupied levels below the Fermi level and redistributed into the deep traps via the conduction band. The occupancy of these traps being larger than in the dark the capture of electrons is lowered in these deep traps. Hence, there remain sufficient electrons for a transit to be observable. In addition, the absorption coefficient is low and the generation of electrons from the continuous light is almost uniform through the sample. The deep traps occupancy is consequently modified through the whole thickness of the crystal. In the case of red light the photon energy (1.9 eV) is not enough to pump electrons from below the Fermi level toward the conduction band and consequently the deep traps occupancy is not modified, at least not enough to give rise to clear transits. Concerning the continuous UV light the photon energy is such that the absorption coefficient is rather high. Indeed, this energy (3.22 eV) is such that band to band generation occurs. Thus, the deep trap occupancy is modified close to the generation electrode but not deeper in the sample that can be considered to be still in the dark. The transient current is larger than in the dark because electrons drift deeper into the crystal as they are not being trapped near the generation electrode, but this current is still continuously decreasing with no particular observable transit because a large part of the back of the sample is still in the dark.

We present in figure 9 typical transients measured at 285 K, with dc blue light illumination, on the BTO:Pb crystal for three different voltages. On figure 9(a) the scales are linear and the currents measured with an applied voltage of 200 and 100 V have been multiplied by a factor of 2 and a factor of 4, respectively. It can be seen that at short time the transients are superimposed and also that, with decreasing voltage, they become much longer. No clear transit time can be deduced from the transients plotted on this linear scale. That is why such a procedure ($\times 2$ for 200 V and $\times 4$ for 100 V) was repeated on figure 9(b) where the transient currents have been plotted on a log–log scale. It appears clearly that the pre-transit parts of all the transients are superimposed following an almost unique slope and that the lower the applied field the farther the onset of the second slope of each transient corresponding to the post-transit regime.

We have used the two tangents methods to estimate the drift mobility from their intersections and found transit times of the order of 2×10^{-5} s, 4×10^{-5} s and 7.2×10^{-5} s for

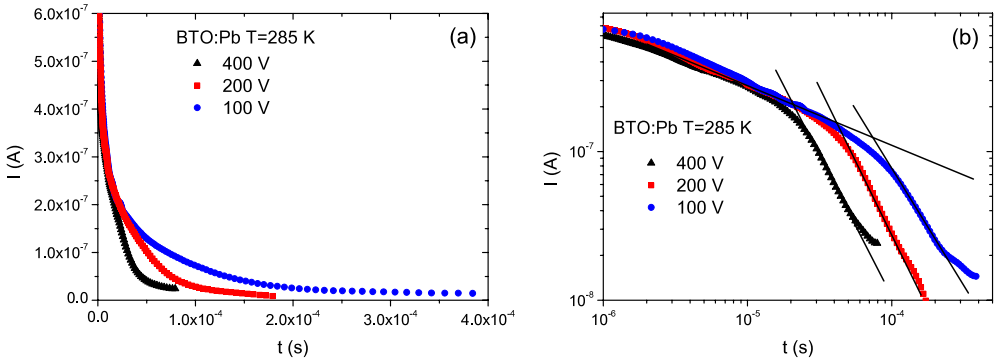

Figure 9. Transients recorded on the BTO:Pb crystal at 285 K for different applied voltages. In (a) they are plotted on linear scales and in (b) they are plotted on a log–log scale. In both figures the transients at 100 and 200 V have been normalized to the transient at 400 V.

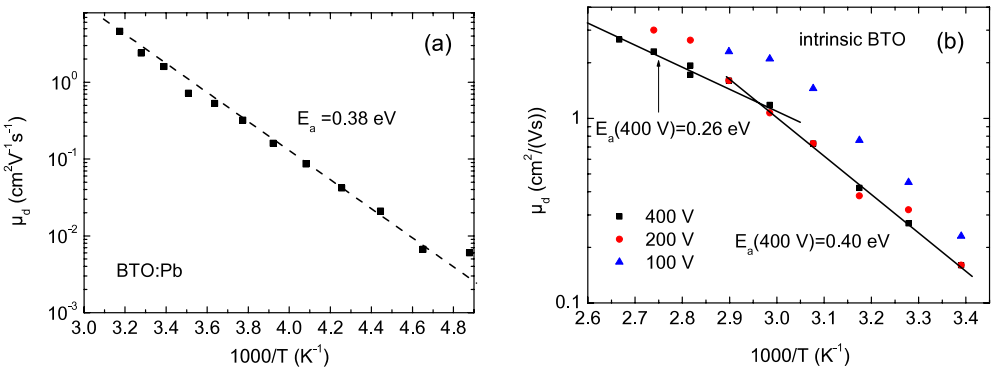

Figure 10. Arrhenius plots of the drift mobilities we recorded at different applied voltages. In (a) for BTO:Pb in which μ_d is almost independent of the bias, and in (b) for undoped BTO.

400, 200 and 100 V, respectively. There is not a universal inverse proportionality between the applied voltage and the transit time, probably because the transients recorded are at the edge between non-dispersive transit and dispersive transit. Indeed, the curve measured at 400 V does not exhibit a clear plateau on the linear scale plot but a rounded shape instead, whereas the curve at 100 V decreases steadily on a linear scale. Hence, the transit at 100 V seems to appear slightly more dispersive than the transit at 400 V. However, at this low bias we cannot reject a possible non-negligible influence of the diffusion that would both result in a smoother transit curve and a proportionately shorter transit time compared with the two other biases as seen in the simulation results. From the above values we estimate the drift mobility at 285 K to be of the order of 0.72 $cm^2\ V^{-1}\ s^{-1}$ for the BTO:Pb crystal.

For both samples we have recorded several transits at different applied voltages and different temperatures. The drift mobilities were found to be activated with temperature and we present in figure 10 the Arrhenius plots for each of the crystals. It clearly appears that the drift mobility measured in the BTO:Pb crystal is much higher (around a factor of 10) than in the intrinsic crystal. It can also be seen that the explored ranges of temperatures are not the same for each crystal. For the BTO:Pb we have not recorded transients above 315 K for we estimated that they would turn out to be too short to be measured accurately at all the different applied biases with our system and for the BTO-J18 we were not able to record transients at low

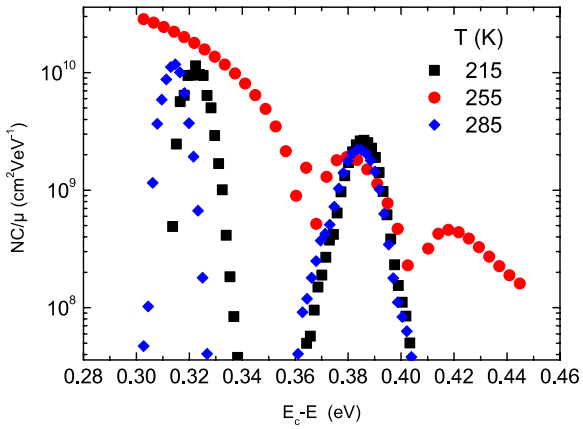

Figure 11. Density of states calculated from a Laplace transform and the Tikhonov regularization procedure applied to several TOF transients. The temperatures of the transients used for this purpose are displayed in the figure.

temperatures (below 280 K) because the transients were too small to be accurately measured. In addition, for this last sample the drift mobility values measured with 100 V applied were always slightly higher (a factor 1.5–2) than with the other biases, though presenting almost the same evolution with temperature. Again we cannot reject a possible influence of the diffusion altering the results when working with this low bias.

4.2. Determination of the density of states

The density of states of the BTO crystals was determined using the method described above applied to various TOF transients. The injected charge (n_{00}) was measured with a fast and calibrated photodiode in place of the sample. Figure 11 summarizes the results obtained for the BTO:Pb crystal in the temperature range 235–295 K. We would like to stress that in figure 11 we do not, strictly speaking, present the DOS versus energy but rather the quantity NC/μ versus energy in which N is the density of states, C the capture coefficient and μ the extended states mobility. This quantity is calculated from equation (10) in which t_0 has been replaced by its expression leading to:

$$\sum_{1}^{m} \frac{\gamma_i \frac{C_n N(E_i)}{\mu} \Delta E}{\left[s+\gamma_i\right]^2} = \frac{Sqn_{00}\xi}{L} \frac{\hat{J}(s)}{B(s)\hat{I}(s)^2}. \tag{13}$$

In this last equation we have neglected the term '-1' present on the right-hand side of equation (10) for it is always much lower than the first term. The advantage of calculating NC/μ instead of N is that all the terms of the right-hand side of equation (13) are determined directly from experimental measurements and data. Consequently, NC/μ, that can be called the reduced density of states (rDOS), is calculated directly from experiment without any scaling parameters such as the C or mobility values that are *a priori* unknown, and direct comparison from one crystal to another is straightforward.

Nevertheless, determination of the DOS or rDOS is only complete when one knows how to scale the energy. A proper scaling of the energy position of a particular defect requires the knowledge of its own attempt-to-escape frequency ν whose value is related to the capture coefficient of the defect. The energy scaling is then made with the expression

$$E_c - E = k_b T \ln(\nu t), \tag{14}$$

t being the time in the studied transient from which the DOS or rDOS is calculated. Usually, ν is unknown and thus one has to make some assumption to plot the rDOS versus energy.

Three different peaks located, respectively, at 0.32 ± 0.01, 0.385 ± 0.01 and 0.42 ± 0.01 eV were detected. One may note again that the shallowest peaks are detected at low temperature and the deepest one at high temperature, the shallowest peaks being broader as it was the case in the simulation study. The energy scale was calculated assuming an attempt-to-escape frequency of $\nu = 10^{12}$ s^{-1}. Concerning the true energy position of the peaks, it is worth underlining that 0.38 eV is precisely the activation energy of the drift mobility we have measured on the same crystal. Hence, though the correspondence between the activation energy of the drift mobility and the energy position of the defect peak is not universal, as mentioned above (see section 3), it here is highly possible that, indeed, there exists in the BTO:Pb crystal a defect level located around 0.38 eV with an attempt-to-escape frequency of precisely the order of 10^{12} s^{-1}. Besides, from the transients obtained with 400 V applied to the intrinsic BTO crystal we have found an activation energy of the mobility of the order of 0.40 eV quite close to the 0.38 eV measured on the BTO:Pb crystal. We are therefore quite confident that in both crystals it exits a defect level located at say 0.39 eV $\pm$ 0.01 eV with $\nu = 10^{12}$ s^{-1}. Concerning the two other peaks found at 0.31 eV and 0.44 eV with $\nu = 10^{+12}$ s^{-1} we cannot claim that these values are exact. We shall come back to this point later.

The NC/μ we have determined from TOF measurements can also be compared to the rDOS we measured on the same crystal by means of the modulated photocurrent (MPC) technique [33–35]. It would take too long to recall all the details of this technique. The basic principle of the MPC is to illuminate a sample in coplanar geometry (as for the TPC) with a flux of light modulated at different frequencies, the photon energy of the light giving rise to band to band generation. The modulus and phase shift of the resulting ac current are measured with a lock-in amplifier, and from these two quantities one can deduce the rDOS distribution in an energy range fixed by the ranges of frequencies and temperatures used during the experiment. Details of the MPC technique applied to BTO crystals are given in [20] and references therein, but we here want to underline that the MPC experiment is strictly the experimental Fourier transform of the TPC technique: MPC measures in the frequency domain what TPC measures in the time domain [18]. Hence, according to the results of our simulations, we should obtain very similar DOS or NC/μ values in the same range of energy from the TOF and MPC techniques.

We present in figure 12 the NC/μ values obtained from the MPC technique. In this figure each set of symbols corresponds to a temperature and each symbol in one set corresponds to a measurement frequency from 12 Hz, for the deepest point in energy in one set, to 40 kHz, for the highest point in energy. The temperatures were varied from 100 to 460 K in 10 K steps and the wavelength of the light was 385 nm. The energy scaling was done assuming an attempt-to-escape frequency $\nu = 10^{12}$ s^{-1} as for the TOF data. Several peaks of defects can be seen with various intensities. A particularly interesting one peaks at 0.31 eV with a large extension towards the deepest energies.

We report in figure 12 the defect peaks detected from TOF measurements, and one can clearly see that the agreement between the three peaks in TOF and the broad one in MPC is quite satisfying. The reason why three peaks are seen in TOF when only one is detected with the MPC technique could be the following. As already mentioned the peak at 0.31 eV detected by MPC is clearly not symmetrical, extending more toward the deepest energies than toward the shallowest. This suggests that this peak is actually made of several ones, particularly in the range 0.31–0.57 eV. Since the MPC technique uses light absorbed near the surface of the crystal whereas in the TOF technique carriers crossing the crystals interact with bulk defects, we believe that, due to the surface proximity, the defect densities measured by the MPC technique

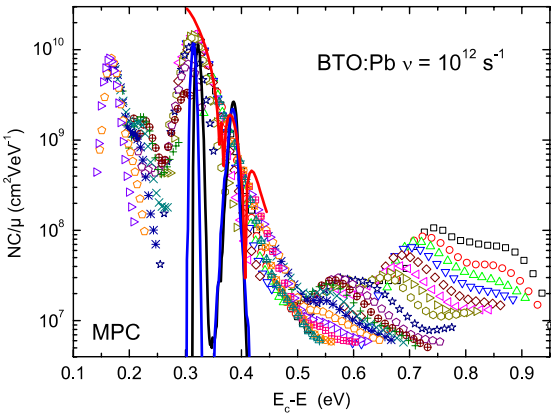

Figure 12. NC/μ versus energy for the BTO:Pb crystal derived from the MPC measurements (symbols). Several peaks of defects can be seen on the explored range of energy. The defect peaks found with the TOF technique (full lines) fit well with the MPC results.

may be enlarged causing different close bulk defect peaks detected by the TOF technique to merge in a single broad one.

Before concluding we would like to say a word on the NC/μ measured on the intrinsic BTO crystal. This quantity was found to be approximately 10 times higher than for the BTO:Pb crystal. Assuming the same extended states mobility for both crystals, it is therefore not surprising to find a drift mobility about 10 times lower for the intrinsic BTO crystal since the trapping rate will be increased by the same factor, and so will the number of trapping events limiting the carrier transport. We can also come back to the determination of the energy position of the peaks. It can be seen in figure 10(b) that the activation energy of the drift mobility of the intrinsic BTO crystals decreases from 0.4 to 0.26 eV at high temperature. This suggests that the defect that limits the electronic transport at high temperature is located around 0.26 eV, and it was apparently not detected from the TOF results. Actually, if one considers the peak positioned at 0.31 eV assuming $\nu = 10^{12}$ s^{-1}, we have demonstrated in [20] that this peak was more probably located at 0.29 ± 0.02 eV with a true attempt-to-escape frequency of the order of $\nu = 2.5 \times 10^{11}$ s^{-1}. It is therefore highly possible that the peak measured at 0.31 eV ($\nu = 10^{12}$) has its maximum around 0.26–0.29 eV with $\nu = 2.5 \times 10^{11}$ s^{-1} and it is indeed detected by the TOF technique.

5. Conclusion

Besides the possibility of studying the mobility of carriers in a given crystal the TOF technique opens up the possibility of determining the density of states interacting with the free carriers during transport. We first proposed an experimental method to apply high voltage pulses on thick crystals in order to ensure a uniform field across the sample during the experiment. Then, by means of numerical simulations, we underlined that the pre-transit regime in TOF was identical to the TPC transient showing that in both techniques the DOS interacting with the free carriers is playing a major role. Hence, we proposed a method for extracting the density of states from the TOF transients. We have also shown that the determination of the transit time by means of two tangents remains the simplest way to extract the drift mobility from a TOF transient since it does not need any ad hoc assumption and the values found fit quite well with those calculated from numerical simulations of the transients.

TOF experiments were performed on two BTO crystals giving very different drift mobilities at room temperature: 2.0 $cm^2\ V^{-1}\ s^{-1}$ for BTO:Pb and 0.21 $cm^2\ V^{-1}\ s^{-1}$ for intrinsic BTO at 300 K. To achieve these measurements we had to superimpose a dc bias of light with a photon energy that must be higher than 2 eV. This indicates that the electronic transport is limited by heavy trapping and a dc bias of light lowers the deep trapping influence.

The rDOS we determine from the TOF measurements compares quite well with the rDOS determined by the MPC technique that is the experimental Fourier transform of the TPC method. Even so, determination of the rDOS by means of the TOF seems more accurate than the MPC method to probe the bulk defects. The characteristics of two defect peaks, energy position and attempt-to-escape frequency, were obtained by combining the results of TOF and MPC. In the range of energy explored by the TOF technique we have found that the rDOS was approximately 10 times higher in the intrinsic BTO crystal than in the BTO:Pb sample. Though we have no appropriate explanation for the origin of this difference, we would like to stress that it explains the differences in the drift mobilities we recorded.

All these developments and results show that the investigation of the transport properties of semiconducting materials needs the combination of different approaches and techniques to obtain a coherent picture, in particular in the determination of the energy position of the defect states.

Acknowledgments

H Belgacem acknowledges support from the Algerian Ministry of Higher Education and Research. Many thanks to J Frejlich and J F Carvalho for providing the BTO crystals.

References

[1] Brinza M, Willekens J, Benkhedir M L, Emelianova E V and Adriaenssens G J 2005 *J. Mater. Sci. Mater. Electron.* **16** 703
[2] Spear W E 1957 *Proc. Phys. Soc.* B **70** 669
[3] Ennouri A, Tapiero M, Vola J P, Zielinger J P, Moisan J Y and Launay J C 1993 *J. Appl. Phys.* **74** 2180
[4] Bloom D and McKeever S W S 1997 *J. Appl. Phys.* **82** 249
[5] Marinova V and Sainov V C 2001 *ROMOPTO 2000: 6th Conf. on Optics* vol 4430 , ed V I Vlad (Belgium: SPIE) pp 483–7
[6] Lecomber P G and Spear W E 1970 *Phys. Rev. Lett.* **25** 509
[7] Marshall J M, Street R A and Thompson J M 1987 *J. Non-Cryst. Solids* **97/98** 563
[8] Abkowitz M 1980 *Phys. Rev.* B **22** 3843
[9] Adriaenssens G J, Seynhaeve G and De Greef S 1985 *J. Non-Cryst. Solids* **77/78** 1187
[10] Scott J C, Pautmeier L Th and Schein L B 1992 *Phys. Rev.* B **46** 8603
[11] Mirchin N R and Peled A 2004 *Holon Academic Inst. Technol. J. Sci. Eng.* **1** 782
[12] Scher H and Montroll E W 1975 *Phys. Rev.* B **12** 2455
[13] Arkhipov V I, Iovu M S, Rudenko A I and Shutov S D 1979 *Phys. Status Solidi* **54** 67
[14] Orenstein J and Kastner M 1981 *Phys. Rev. Lett.* **46** 1421
[15] Tiedje T and Rose A 1980 *Solid State Commun.* **37** 49
[16] Schmidlin F W 1977 *Phys. Rev.* B **16** 2362
[17] Longeaud C, Fournet G and Vanderhaghen R 1988 *Phys. Rev.* B **38** 7493
[18] Seynhaeve G F, Barclay R P, Adriaenssens G J and Marshall J M 1989 *Phys. Rev.* B **39** 10196
[19] Main C 2002 *J. Non-Cryst. Solids* **299–302** 525
[20] Nagase T, Kishimoto K and Naito H 1999 *J. Appl. Phys.* **86** 5026
[21] Frejlich J, Montenegro R, Inocente-Junior N R, Dos Santos P V, Launay J C, Longeaud C and Carvalho J F 2007 *J. Appl. Phys.* **101** 043101
[22] Prokofiev V V, Carvalho J F, Andreeta J P, Gallo N J H, Hernandes A C, Frejlich J, Freschi A A, Garcia P M, Maracaiba J, Kamshilin A A and Jaaskelainen T 1995 *Cryst. Res. Technol.* **30** 171
[23] Vanderhaghen R 1988 *Phys. Rev.* B **38** 10755

[24] Scott J C, Pautmeier L Th and Schein L B 1992 *Phys. Rev.* B **46** 8603
[25] Main C, Brüggemann R, Webb D P and Reynolds S 1992 *Solid State Commun.* **83** 401
[26] Belgacem H, Merazga A and Longeaud C 2005 *Semicond. Sci. Technol.* **20** 56
[27] Main C, Reynolds S, Gueorguieva M and Badran R I 2001 Materials for information technology in the new millenium *ISCMPII: Proc. 11th Int. School on Condensed Matter Physics* ed J M Marshall *et al* (Bath: Bookcraft) pp 8–17
[28] Marshall J M 2000 *Phil. Mag.* B **80** 1705
[29] Noolandi J 1977 *Phys. Rev.* B **16** 4466
[30] Muller-Horsche E, Haarer D and Scher H 1987 *Phys. Rev.* B **35** 1273
[31] Wendlandt M 2006 Non linear constraint smooth regularization, Matlab website http://www.mathworks.com/matlabcentral/fileexchange/loadFile.do?objectId=7712&objectType=FILE
[32] Brancik L 1999 Programs for fast numerical inversion of laplace transforms in matlab language environment *Konf. MATLAB 99 (ZCU, Plzen, Germany)* pp 27–39
[33] Oheda H 1981 *J. Appl. Phys.* **52** 6693
[34] Longeaud C and Kleider J P 1992 *Phys. Rev.* B **45** 11672
[35] Brüggemann R, Main C, Berkin J and Reynolds S 1990 *Phil. Mag.* B **62** 29